

# Gravitational lensing statistics with extragalactic surveys

## I. A lower limit on the cosmological constant

Ralf Quast<sup>1</sup> and Phillip Helbig<sup>2</sup>

<sup>1</sup> Universität Hamburg, Hamburger Sternwarte, Gojenbergsweg 112, D-21029 Hamburg, Germany

<sup>2</sup> University of Manchester, Nuffield Radio Astronomy Laboratories, Jodrell Bank, Macclesfield, Cheshire SK11 9DL, England

Received 2 December 1998 / Accepted 14 January 1999

**Abstract.** We reanalyse optical gravitational lens surveys from the literature in order to determine relative probabilities in the  $\lambda_0$ - $\Omega_0$  plane, using a softened singular isothermal sphere lens model. In addition, we examine a portion of the  $\lambda_0$ - $\Omega_0$  plane which includes all viable cosmological models; this is vital for comparison with other cosmological tests. The results are, within the errors, consistent with those of more specialised analyses, such as those concerning upper limits on  $\lambda_0$  in a flat universe. We note that gravitational lensing statistics can provide a quite robust *lower* limit on the cosmological constant as well, which could prove important in confirming current claims of a positive cosmological constant. At 95% confidence, our lower and upper limits on  $\lambda_0 - \Omega_0$ , using lens statistics information alone, are respectively  $-3.17$  and  $0.3$ . For a flat universe, these correspond to lower and upper limits on  $\lambda_0$  of respectively  $-1.09$  and  $0.65$ .

**Key words:** gravitational lensing – cosmology: theory – cosmology: observations

---

### 1. Introduction

The use of gravitational lensing statistics as a cosmological tool was first considered in detail by Turner et al. (1984); the influence of the cosmological constant was investigated thoroughly by Fukugita et al. (1992), building on the work of Turner (1990) and Fukugita et al. (1990). More recently, Kochanek (1996, hereafter K96, and references therein) and Falco et al. (1998) have laid the groundwork for using gravitational lensing statistics for the detailed analysis of extragalactic surveys. However, these analyses either have concentrated on a small subset of the possible cosmological models as described by the density parameter  $\Omega_0$  and the cosmological constant  $\lambda_0$ , have used a simpler (singular) lens model or both. This analysis is the first time

---

*Send offprint requests to:* R. Quast

*Correspondence to:* rquast@hs.uni-hamburg.de

$\lambda_0$  and  $\Omega_0$  have been used as independent parameters in conjunction with a non-singular lens model in an analysis of this type, complementing similar analyses with other emphases. (See Cheng & Krauss (1999) for a discussion of the importance of including a core radius.) Also, we include enough of the  $\lambda_0$ - $\Omega_0$  plane to avoid neglecting any possibly viable models; this also makes the comparison with a variety of other cosmological tests easier. This is especially important in light of the fact that many analyses (e.g. Perlmutter et al. 1998; Riess et al. 1998; Schmidt et al. 1998; Carlberg et al. 1998a; Lineweaver 1998; Guerra et al. 1998; Daly et al. 1998) are now suggesting that our universe may contain a significant cosmological constant *and* be non-flat.

The plan of this paper is as follows. Sect. 2 reviews the groundwork and serves to define our notation. In Sect. 3 we specify the observational data and selection functions we use and formulate prior information about the parameters  $\lambda_0$  and  $\Omega_0$ . Sect. 4 describes the parametric submodels we use and the numerical computations we perform. In Sect. 5 we discuss our results and compare them with others. Sect. 6 presents our summary and conclusions.

### 2. Probability of multiply imaged sources

In this section we briefly review the statistical concepts introduced in K96; this also serves to define our notation. Note that with regard to cosmological notation we follow that of Kayser et al. (1997), repeating here only 2 equations needed for discussion in this paper: the comoving spherical volume element at redshift  $z$  reads

$$dV = 4\pi r^2 \frac{c}{H_0} \frac{dz}{\sqrt{Q(z)}}, \quad (1)$$

where

$$Q(z) = \Omega_0(1+z)^3 - (\Omega_0 + \lambda_0 - 1)(1+z)^2 + \lambda_0. \quad (2)$$

Following the K96 approach, we assume that the light deflection properties of the gravitational lenses can be modelled with a particular type of circularly symmetric lens models with a monotonically declining radial mass

have two critical radii on which the magnification diverges (e.g. Schneider et al. 1992). It is possible to estimate the probability  $p(m, z_s)$  of the event

*A source at redshift  $z_s$  is triply imaged. The total apparent magnitude of the three images is  $m$ . The image configuration meets the selection criteria  $S$  and, particularly, shows the properties  $C$ .*

If the outer and inner critical angular radii of the lens potential are respectively  $r_+$  and  $r_-$ , the image magnification at radial angular position  $r$  is  $\mu(r)$ , the total magnification of the three images of a source at angular position  $y$  is  $M(y)$ , the functions  $S(y)$  and  $C(y)$  are 0|1 valued selection functions, the comoving density of lenses of luminosity  $L$  is  $dn/dL$  and the number-magnitude counts of sources are  $dN/dm$ , then

$$p(m, z_s) = \frac{1}{2} \int_0^{z_s} \frac{dV}{dz} \int_0^\infty \frac{dn}{dL} \int_{r_-}^{r_+} r |\mu(r)|^{-1} \times \underbrace{B(m, z_s, y) S(y) C(y)}_{\text{selection}} dr dL dz, \quad (3)$$

where

$$B(m, z, y) = \frac{dN}{dm} \{m + 2.5 \log[M(y)], z\} \left[ \frac{dN}{dm}(m, z) \right]^{-1}. \quad (4)$$

The critical radii, the image magnifications and the source position are functions of the lens model, the luminosity of the lens galaxy and the redshifts of the source and the lens galaxy. If the underbraced functions are dropped, Eq. (3) yields the optical depth – the fraction of the sky included within the caustics of all lenses between us and the sources at redshift  $z_s$ . The inclusion of these functions accounts for magnification bias, survey selection effects (including what is defined as a lensing event) and allows the observed image separation to be taken into account.

Equation (3) parametrically depends on  $\lambda_0$  and  $\Omega_0$  through Eq. (1) and through the angular size distances,<sup>1</sup> which are needed for calculating observable quantities from the lens model (these also depend on the source and lens redshifts). Equation (3) additionally depends on parametric submodels required to model the lens population and the number-magnitude counts of sources. Since throughout this paper we are principally interested in  $\lambda_0$  and  $\Omega_0$ , hereafter we refer to the submodel parameters as nuisance parameters (although technically they are on the same footing with  $\lambda_0$  and  $\Omega_0$ , there are not of as much interest here and thus a nuisance). In principle, one could also incorporate other observables into the parametric model; the reasons for not doing so are practical.

<sup>1</sup> In general, the angular size distances depend not only on  $\lambda_0$  and  $\Omega_0$  but on the degree of homogeneity in the universe as well (see, e.g., Kayser et al. 1997). However, in contrast to some other cosmological tests, this effect is relatively unimportant for the type of analysis performed here (see, e.g., Fukugita et al. 1992).

can numerically compute Eq. (3) and reasonably estimate the probability  $1 - p(m_i, z_i)$  that the quasar  $i$  is singly imaged or the probability  $p(m_i, z_i, \theta_i)$  that the quasar  $i$  is multiply imaged and its images (within some tolerance) are separated by  $\theta_i$ . If the survey data  $D$  contains  $M$  singly and  $N$  multiply imaged quasars, we can estimate the probability of the event

*In a model universe fixed by the cosmological parameters  $\lambda_0$ ,  $\Omega_0$  and the nuisance parameters  $\xi$ , a multiply imaged quasar survey collects the observational data  $D$ .*

by applying the parametric model (or likelihood function)

$$\ln[p(D|\Omega_0, \lambda_0, \xi)] = - \sum_{i=1}^M p(m_i, z_i) + \sum_{j=1}^N \ln[p(m_j, z_j, \theta_j)], \quad (5)$$

where the logarithm  $\ln[1 - p(m_i, z_i)]$  was expanded to first order. We can combine surveys of different objects by adding the logarithms of the likelihood functions for the individual surveys, and can combine surveys containing the same objects by applying their joint selection function.

In Bayesian theory the model parameters  $\lambda_0$ ,  $\Omega_0$ ,  $\xi$  are regarded as random quantities with known joint prior probability density function  $p(\lambda_0, \Omega_0, \xi)$ . Applying Bayes's theorem, the appropriate posterior probability distribution given the observational data  $D$  is

$$p(\lambda_0, \Omega_0, \xi|D) = p(D|\lambda_0, \Omega_0, \xi) \otimes p(\lambda_0, \Omega_0, \xi), \quad (6)$$

where the operation ' $\otimes$ ' denotes multiplication followed by normalisation. Marginalising the nuisance parameters

$$p(\lambda_0, \Omega_0|D) = \int p(\lambda_0, \Omega_0, \xi|D) d\xi. \quad (7)$$

yields the (marginal) posterior probability density function for the parameters  $\lambda_0$  and  $\Omega_0$ . In the limit where all nuisance parameters take a precise value,  $\xi = \xi_0$ , the joint prior probability density function  $p(\lambda_0, \Omega_0, \xi)$  factorises into  $p(\lambda_0, \Omega_0)$  and a delta distribution  $\delta(\xi - \xi_0)$ , and Eq. (7) simplifies to

$$p(\lambda_0, \Omega_0|D) = p(D|\lambda_0, \Omega_0, \xi_0) \otimes p(\lambda_0, \Omega_0). \quad (8)$$

On the basis of Eq. (7) or Eq. (8), we can calculate confidence regions for two parameters or perform further marginalisations and calculate mean values, standard deviations and marginal confidence intervals for one parameter.

### 3. Observational data and prior information

We use the observational data of the optical multiply imaged quasar surveys by Crampton et al. (1992), Jaunsen et al. (1995), Kochanek et al. (1995), Yee et al. (1993) and the observational data of the HST Snapshot Survey

tained in the sample. The magnitudes are V magnitudes unless otherwise specified. The image separations are taken from Kochanek et al. (1997)

| Identifier  | $m$ [mag] | $z_s$ | $\theta$ ["] |
|-------------|-----------|-------|--------------|
| Q 0142-100  | 17.0      | 2.72  | 2.2          |
| Q 1009-0252 | 18.1 B    | 2.74  | 1.5          |
| Q 1115+080  | 16.2      | 1.72  | 2.2          |
| Q 1208+1011 | 17.9      | 3.80  | 0.48         |
| Q 1413+117  | 17.0      | 2.55  | 1.2          |

compiled by Maoz et al. (1993), including Q 0142-100, Q 1115+080 and Q 1413+117. If applicable, we replace the apparent quasar V magnitude catalog data found in Crampton et al. (1992), Jaunsen et al. (1995) and Yee et al. (1993) with more current data from Veron-Cetty & Veron (1996). We estimate the Kochanek et al. (1995) apparent quasar V magnitude data by adding the survey average V-R and V-I colours to the observational R and I magnitude data. Following K96, we only include quasars with redshift  $z_s > 1$ . In all, our sample contains 807 singly and 5 multiply imaged quasars. The observational data of the multiply imaged quasars are summarised in Table 1. Our complete input data can be obtained from

[http://multivac.jb.man.ac.uk:8000/ceres/data\\_from\\_papers/lower\\_limit.html](http://multivac.jb.man.ac.uk:8000/ceres/data_from_papers/lower_limit.html)

This follows K96 for purposes of comparison. Since much larger surveys (i.e. CLASS) will be considered in a future paper, there is little point in increasing the number of lenses for its own sake. Since radio observations are considered in more detail in a companion paper (Helbig et al. 1999), we restrict ourselves to optical surveys in this paper. We use the Crampton et al. (1992), HST Snapshot Survey and Yee et al. (1993) survey selection functions proposed in Kochanek (1993), the Jaunsen et al. (1995) survey selection function at 1'' seeing and the preliminary Kochanek et al. (1995) survey selection function.

Before considering prior information in more detail, one must first decide which region of the  $\lambda_0$ - $\Omega_0$  plane is to be investigated. Clearly, this region should be defined by either exact constraints or conservative estimates, as opposed to current ‘best fit’ values (and their errors), in order to avoid excluding any possibly viable cosmological models. Also, it is desirable for the region to be on the large side, so that in addition the sensitivity of the test (i.e. what regions of the  $\lambda_0$ - $\Omega_0$  plane can be ruled out at a high confidence level) can be investigated.

### 3.1. The range of $\Omega_0$ and $\lambda_0$

The mass clustered with galaxies on smaller scales,  $\Omega_{0,\text{gal}}$ , is 0.1 within a factor of two (e.g. Peebles 1993). This lower limit is small compared to our full  $\Omega_0$  range so we do not assume any prior lower limit on  $\Omega_0$  except, of course,  $\Omega_0 \geq 0$ . (9)

to note that, within the framework of cosmological models based on general relativity with which we (and almost everyone else at present) are working,  $\Omega_0 \geq 0$  is a *requirement*. Results reported which include  $\Omega_0 < 0$  within the errors, or even as a best-fit value, do not indicate ‘implausible results’ but merely improper statistics. Often, confidence contours are assumed to be ellipses and these are extended, if applicable, to  $\Omega_0 < 0$ . (Of course, it is possible that  $\Omega_0 = 0$  is within the errors or even the best fit value for a certain set of results.)

An extremely conservative upper limit comes from dynamical tests on larger (though still cosmologically small) scales; when this work was started, we assumed an (again, extremely conservative) upper limit  $\Omega_0 \leq 2$  (Czoske 1995). Since then, these methods have started to indicate smaller values of  $\Omega_0$ , (e.g. da Costa et al. 1998) more in line with both a long tradition of low  $\Omega_0$  values (e.g. Gott et al. 1974; Coles & Ellis 1994, 1997) (albeit with somewhat larger errors) as well as new determinations (often with quite small errors), examples of which are mentioned in Sect. 3.2.

We have assumed no prior upper or lower limits on  $\lambda_0$  per se. This has two reasons:

- ‘Direct’ measurements of  $\lambda_0$  (as opposed to measurements of a combination of parameters involving  $\lambda_0$ ) are virtually nonexistent.
- We obtain a small enough range in  $\lambda_0$  from the values obtained from joint constraints on the range of  $\Omega_0$  and  $\lambda_0$ .

Historically, positive  $\lambda_0$  values have been considered more than negative ones, probably because positive values can have a wide range of relatively easily observable effects, while negative ones are more difficult to measure. Many cosmological tests have a degeneracy such that  $\lambda_0$  and  $\Omega_0$  are correlated, so that increasing  $\lambda_0$  can be compensated for in some sense by increasing  $\Omega_0$  as well. Thus, effects of negative values of  $\lambda_0$  for a given value of  $\Omega_0$  are hard to differentiate from the effects of larger values of  $\Omega_0$  for larger (less negative) values of  $\lambda_0$  or even  $\lambda_0 = 0$ .

Here, we consider negative values of  $\lambda_0$  as well. There is no a priori reason why they cannot exist. *If* one believes that the ‘source’ of  $\lambda_0$  are zero-point fluctuations of a quantum vacuum, this would lend support to the idea that  $\lambda_0 > 0$ . However, it is not clear that this *must* be the *only* source of  $\lambda_0$ , and indeed it has been argued that, if this source of  $\lambda_0$  exists, there must be an additional contribution with a *negative* value (e.g. Martel et al. 1998, though the assumption that this is possible is so obvious to the authors it is barely stated!).

In spatially closed ( $k = +1$ ) models, the antipode is required to be at  $z > 4.5$ , the redshift of the most redshifted multiply imaged object currently known (Gott et al. 1989;

panel in the middle of the left column of Fig. 1 marks the right side of the region thus enclosed. This gives us a slightly  $\Omega_0$ -dependent upper limit on  $\lambda_0$  which is slightly stronger than that obtained by merely excluding models with no big bang. (This can be done because these models have a maximum redshift which is less than the redshift of high-redshift objects, the only exception being some cosmological models which have  $\Omega_0 < 0.05$ , the robust lower limit discussed above (e.g. Feige 1992).)

The age of the universe in units of the Hubble time,  $H_0^{-1}$ , is

$$\tau_0 = \int_0^\infty \frac{dz}{(1+z)\sqrt{Q(z)}}, \quad (10)$$

where  $Q(z)$  is given by Eq. (2) and thus depends on  $\Omega_0$  and  $\lambda_0$ . (There are world models in which the maximum redshift is not infinite but these are all models without a big bang and are excluded by the constraint from the antipodal redshift or the lower limit on  $\Omega_0$  as discussed above and are thus not relevant for this work.) Clearly, in any physically realistic world model,  $\tau_0 H_0^{-1}$  exceeds the age of the oldest galactic globular clusters:

$$\tau_0 > t_{\text{gc}} H_0. \quad (11)$$

Following Carroll et al. (1992), we take a robust lower limit on  $\lambda_0$  from conservative lower limits on the Hubble constant and age of the universe. This gives a lower limit on  $\lambda_0$  from the value at  $\Omega_0 = 0$ ; at larger values of  $\Omega_0$  the constraint on  $\lambda_0$  is not as strict—by assuming the lower limit of  $\lambda_0 = -5$  independent of  $\Omega_0$  we are being conservative. We choose  $\lambda_0 \geq -5$  instead of  $\lambda_0 \geq -7$  as in Carroll et al. (1992) since no published current constraints examine this region in detail. (Were this the case, then including this area would be helpful if only to aid a direct comparison.) This value corresponds roughly to the *one-sided* 99% confidence level in the top row of Fig. 1 (see Sect. 3.2), which is also a reason not to extend the area to more negative  $\lambda_0$  values.

### 3.2. Prior probability for $\lambda_0$ and $\Omega_0$

We have assumed no prior knowledge of  $\lambda_0$  per se, apart from the upper and lower limits discussed above. This has three reasons:

- ‘Direct’ measurements of  $\lambda_0$  (as opposed to measurements of a combination of parameters involving  $\lambda_0$ ) are virtually nonexistent.
- Based on general knowledge from the literature and our own low-resolution calculations, we expect lens statistics itself to constrain  $\lambda_0$  quite well.

<sup>2</sup> Recently, a lensed object of even larger redshift has been detected at  $z = 4.92$  (Franx et al. 1998). However, at our resolution this would make only a negligible difference to the results so we have not updated the calculations to reflect this.

(Sect. 5), the value of  $\lambda_0$  is observationally not as well established as that of  $\Omega_0$ .

Regarding  $t_{\text{gc}}$  and  $H_0$  as independent random quantities with known prior probability density functions  $p(t_{\text{gc}})$  and  $p(H_0)$ , the probability that Eq. (11) is satisfied is

$$P(\tau_0 > t_{\text{gc}} H_0) = \int_0^\infty p(H_0) \int_0^{\tau_0/H_0} p(t_{\text{gc}}) dt_{\text{gc}} dH_0. \quad (12)$$

A cosmological world model is compatible with the absolute age of the oldest galactic globular clusters as long as the above expression does not vanish. Reasonably, we assume a prior probability density function that is proportional to this expression

$$p_1(\lambda_0, \Omega_0) = 1 \otimes \int_0^\infty p(H_0) \int_0^{\tau_0/H_0} p(t_{\text{gc}}) dt_{\text{gc}} dH_0. \quad (13)$$

The best estimate of the absolute age of the oldest galactic globular clusters currently is  $t_{\text{gc}} = 11.5 \pm 1.3$  Gyr (Chaboyer et al. 1998). We choose to formulate this prior information in the form of a lognormal distribution that meets these statistics

$$p(t_{\text{gc}}) = L(t_{\text{gc}} | 11.5 \text{ Gyr}, 1.3 \text{ Gyr}). \quad (14)$$

Similarly, we roughly estimate  $H_0 = 65 \pm 10 \text{ km s}^{-1} \text{ Mpc}^{-1}$  and choose to formulate this prior information in form of a normal distribution

$$p(H_0) = N(H_0 | 65 \text{ km s}^{-1} \text{ Mpc}^{-1}, 10 \text{ km s}^{-1} \text{ Mpc}^{-1}), \quad (15)$$

where the notation for  $L$  and  $N$  is such that the two arguments correspond to the mean and standard deviation.

This estimate is compatible with ‘small’ values of the Hubble constant, which is conservative in the sense that it restricts our region of the  $\lambda_0$ - $\Omega_0$  plane less than would ‘large’ values. By the same token we neglect any time between the big bang and the formation of the oldest globular clusters. Inserting Eq. (14) and Eq. (15) in Eq. (13) one obtains a well-founded a priori probability distribution for the parameters  $\Omega_0$  and  $\lambda_0$ .

Although observational evidence has always indicated a low value of  $\Omega_0$  (e.g. Gott et al. 1974; Coles & Ellis 1994, 1997), the inflationary paradigm (e.g. Guth 1981), coupled with a prejudice against a non-negligible value of  $\lambda_0$ , has created a prejudice in favour of  $\Omega_0 = 1$ ,<sup>3</sup> unfortunately too often to the extent where this prior belief has been elevated to the status of dogma (see, e.g., Matravers et al. 1995, for an illuminating account) even though there are serious fundamental problems with the inflationary idea (e.g. Penrose 1989) and even though there might be other solutions to the problems it claims to solve (e.g. Barrow

<sup>3</sup> After this was found to conflict with too many observations, the prejudice against a non-negligible value of  $\lambda_0$  weakened, and the new prejudice has been in favour of a flat universe with  $\lambda_0 + \Omega_0 = 1$ .

tionary thinking (e.g. Turok & Hawking 1998) seems able to predict values for  $\lambda_0$  and  $\Omega_0$  similar to current observationally determined values, though it would have been more interesting had this prediction been made before the recent improvements in the observational situation. (To be fair, many leading practitioners of inflation consider a flat universe to be a robust prediction and its observational falsification essentially a falsification of the entire paradigm.) Recently, in the light of overwhelming observational evidence in favour of a low value of  $\Omega_0$  (e.g. Carlberg et al. 1998b; Carlberg 1998; Carlberg et al. 1998c; Bahcall 1998; Bahcall et al. 1997; Fan et al. 1997; Bartelmann et al. 1998; Lineweaver 1998), whether determined more or less independently or in combination with other parameters, this prejudice is starting to weaken. Conservatively, these results can be summarised as

$$p_2(\lambda_0, \Omega_0) = L(\Omega_0|0.4, 0.2). \quad (16)$$

A prior constraint on  $\Omega_0$  is useful since lensing statistics alone, as expected and as our results show, cannot usefully constrain  $\Omega_0$ .

In addition, we also consider the product of  $p_2(\lambda_0, \Omega_0)$  with the age constraint  $p_1(\lambda_0, \Omega_0)$ ,

$$p_3(\lambda_0, \Omega_0) = p_1(\lambda_0, \Omega_0) \otimes p_2(\lambda_0, \Omega_0). \quad (17)$$

### 3.3. General discussion of prior information

Using harsher constraints would mean that results would reflect almost exclusively the prior information as opposed to the information derived from lensing statistics. It is not the purpose of this paper to do a joint analysis of several cosmological tests,<sup>4</sup> but rather to examine lens statistics as a cosmological test. For practical reasons, an upper limit on  $\Omega_0$  and upper and lower limits on  $\lambda_0$  are required. On the other hand, it is sensible to combine the results with conservative constraints from other well-understood cosmological tests where there is general agreement and little room for debate. Within our upper and lower limits, we present our results both with and without the constraints discussed above. The density values and confidence contours of the three prior probability density functions are shown in the right column of Fig. 1.

## 4. Calculations

Following K96, we use the Hinshaw & Krauss (1987) softened isothermal sphere model for modeling the light deflection properties of the lens galaxies. For this model, the lens equation reads

$$x - y = \frac{bx}{\hat{s} + \sqrt{x^2 + \hat{s}^2}}, \quad (18)$$

<sup>4</sup> but see Sect. 5

gular position in the source plane,  $b \equiv 4\pi(\sigma/c)^2(D_{\text{ds}}/D_{\text{os}})$ ,  $\sigma$  denotes the one-dimensional velocity dispersion of the dark matter,  $s$  denotes the core radius,  $\hat{s} \equiv s/D_{\text{od}}$  is the angular core radius and  $D_{\text{od}}$ ,  $D_{\text{os}}$  and  $D_{\text{ds}}$  denote the angular size distances between the observer and the lens galaxy, the observer and the source and the lens galaxy and the source, respectively. Still following K96, we model the distribution of elliptical and lenticular lens galaxies using Schechter functions with constant comoving density

$$n_e = 0.61 \pm 0.21 h^3 10^{-2} \text{ Mpc}^{-3} \quad (19)$$

( $h = H_0 10^{-2} \text{ km}^{-1} \text{ s Mpc}$ ) and slope

$$\alpha_e = -1.0 \pm 0.15. \quad (20)$$

The lens galaxy luminosities are converted to the dark matter velocity dispersions of the softened isothermal lens model by means of Faber–Jackson type relations,

$$L/L_{*e} = (\sigma/\sigma_{*e})^{\gamma_e}, \quad (21)$$

where

$$\gamma_e = 4.0 \pm 0.5 \quad (22)$$

and

$$\sigma_{*e} = 225.0 \pm 22.5 \text{ km s}^{-1}. \quad (23)$$

The core radii of the softened isothermal lens model are varied with the dark matter velocity dispersions according to

$$s/s_{*e} = (\sigma/\sigma_{*e})^{2+\varepsilon}, \quad (24)$$

where  $\varepsilon = 2.8$  and  $s_{*e} = 10h^{-1} \text{ pc}$ . We consider elliptical and lenticular lens galaxies only. For the number-magnitude counts of quasars, we adopt the best-fit model from K96. We neglect here evolution, dust and other possible systematic effects and refer the reader to K96 for a discussion.

In our first calculations we apply Eq. (8) and compute the a priori likelihood

$$p(D|\lambda_0, \Omega_0, \xi_0) \quad (25)$$

and the posterior probability density functions

$$p_1(\lambda_0, \Omega_0|D) = p(D|\lambda_0, \Omega_0, \xi_0) \otimes p_1(\lambda_0, \Omega_0), \quad (26)$$

$$p_2(\lambda_0, \Omega_0|D) = p(D|\lambda_0, \Omega_0, \xi_0) \otimes p_2(\lambda_0, \Omega_0), \quad (27)$$

and

$$p_3(\lambda_0, \Omega_0|D) = p(D|\lambda_0, \Omega_0, \xi_0) \otimes p_3(\lambda_0, \Omega_0) \quad (28)$$

in the limit where all nuisance parameters take precisely their mean values. To obtain an impression of the consequences of neglecting the uncertainties of the nuisance parameters, in our second calculation we increase the value of the most uncertain nuisance parameter,  $n_e$ , by two standard deviations.

For the computation of the innermost integral on the right side of Eq. (3), we consider the detectability of images in pairs: If the separation between the two closest images – these are always images 2 and 3, counting from

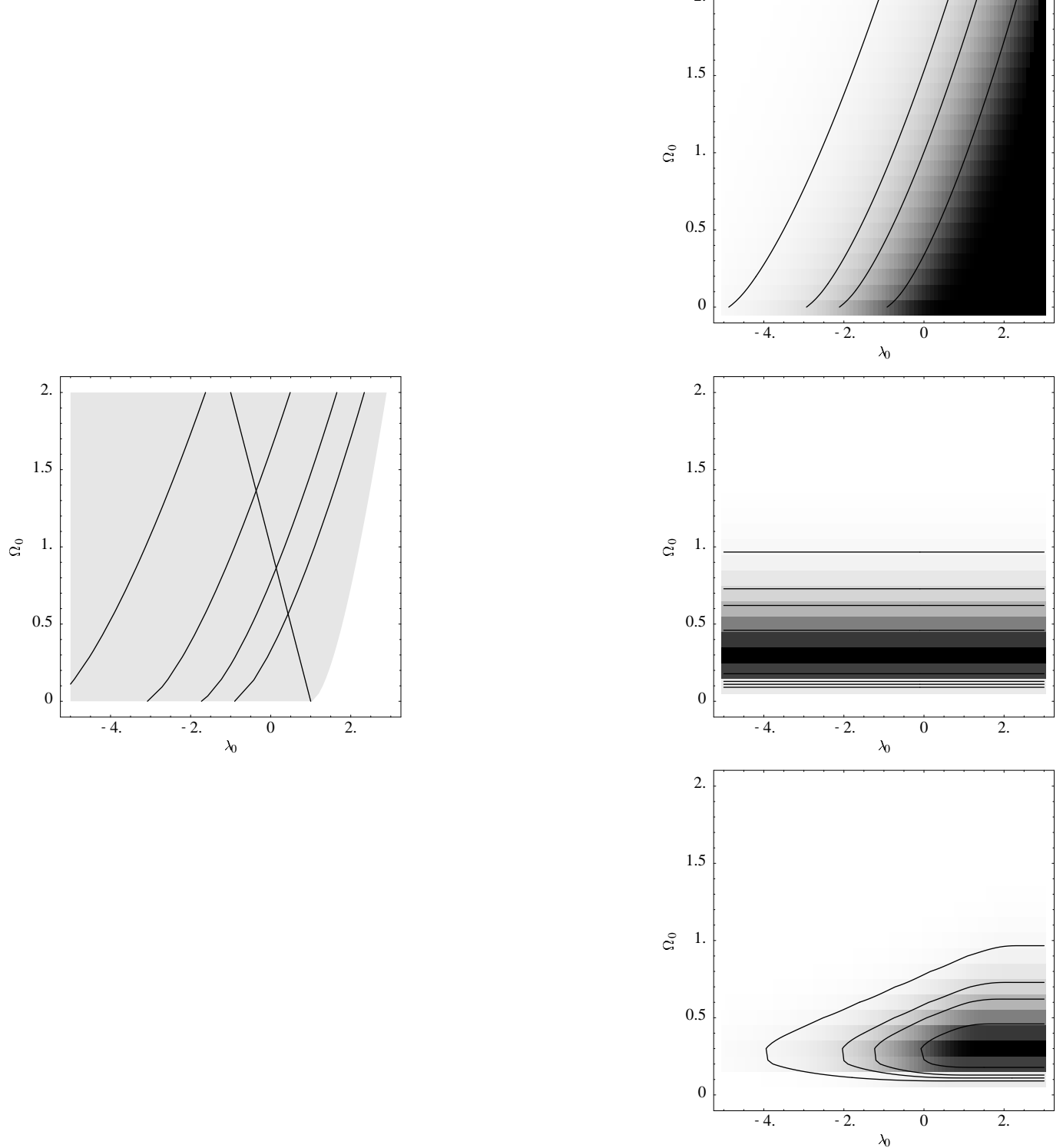


**Fig. 1.** *Left column:* The cosmological parameter plane. The four curved lines in the plot at the left are the isochrones  $t_0 H_0 = 0.5, \dots, 0.8$ . The straight line marks spatially flat world models. In the white region, the antipodal redshift falls below  $z = 4.5$ , the redshift of the most redshifted multiply imaged object currently known (Gott et al. 1989; Park & Gott 1997). *Right column:* The prior probability distributions  $p_1(\lambda_0, \Omega_0)$  (top panel),  $p_2(\lambda_0, \Omega_0)$  (middle panel) and  $p_3(\lambda_0, \Omega_0)$  (bottom panel). The pixel grey level is directly proportional to the probability density ratio, darker pixels reflect higher ratios. The pixel size reflects the resolution of our numerical computations. The contours mark 0.61, 0.26, 0.14 and 0.036 of the peak likelihood for the parameters  $\lambda_0$  and  $\Omega_0$ , which would correspond to the boundaries of the minimum 0.68, 0.90, 0.95 and 0.99 confidence regions *if the distribution were Gaussian*

vey resolution limit  $S(y)$ , we define the image separation and flux ratio for the purpose of sample selection based on the two brightest images, usually 1 and 2. Otherwise we construct one image from the combined fluxes and flux-weighted positions of images 2 and 3 and define the image separation and flux ratio for the purpose of sample selection based on this combination image and image 1.

In general, if the separation between images 1 and 2 is too large for the survey *and* the separation between images 2 and 3 is large enough, then the image separation and flux ratio for the purpose of sample selection should be based on images 2 and 3. However, the present surveys are sensitive to the largest separations due to isolated galaxies, so this case doesn't need to be addressed in this paper (i.e. implementing it would lead to the same results in the present case).

For the calculation of the probabilities  $p(m_i, z_i, \theta_i)$  the function  $C(y)$  selects only those image configurations whose separation is  $\pm 10$  per cent of the observed separation  $\theta_i$ .

Each of the three integrals on the right side of Eq. (3) is approximated to an accuracy better than 0.004 by a family of recursive monotone stable formulae (Favati et al. 1991a,b).

## 5. Results and discussion

### 5.1. Information content

Given some observational data  $D$ , some model parameters  $\phi$ , and some prior and posterior probability density functions  $p(\phi)$  and  $p(\phi|D)$ , the amount of information obtained from the data (e.g. Bernardo & Smith 1994) (on a logarithmic scale) is

$$\log[I(D)] = \int p(\phi) \log \left[ \frac{p(\phi|D)}{p(\phi)} \right] d\phi. \quad (29)$$

The amounts of information obtained from our sample data are given in the caption of Fig. 3.

### 5.2. Results

The left panel of Fig. 2 shows the constraints on the cosmological parameters  $\lambda_0$  and  $\Omega_0$  based only on the information obtained from the lens statistics.

Quite good constraints can be placed on  $\lambda_0$ , more or less independent of  $\Omega_0$ . It is a well-known fact (see K96 and references therein) that lensing statistics can provide a good *upper* limit on  $\lambda_0$ . While in the past this has mainly been discussed in the context of flat cosmological models, it is of course more general (Carroll et al. 1992; Falco et al. 1998). Although no unexpected effects are seen, it is important to note that this is the first time  $\lambda_0$  and  $\Omega_0$  have been used as independent parameters in conjunction with a non-singular lens model in an analysis of this type.

lensing statistics can place a quite firm *lower* limit on  $\lambda_0$  as well, again more or less independent of  $\Omega_0$ . The constraint is not as tight since the gradient in the probability density is not as steep towards negative  $\lambda_0$  as towards positive  $\lambda_0$ . If this lower limit can be improved enough, it could provide an independent confirmation of the detection of a positive cosmological constant (see Sect. 5.3). On the other hand, this might be difficult, since Poisson errors in the number of lenses and uncertainties in the normalisation of the luminosity density of galaxies introduce relatively large uncertainties in this region of parameter space (K96, Falco et al. 1998). The latter effect is illustrated in the right panel of Fig. 2, where  $n_e$ , the galaxy luminosity density normalisation, is increased by two standard deviations: the derived lower limit on  $\lambda_0$  changes much more than does the upper limit. Nevertheless, our robust lower limit is much better than the  $-7$  mentioned in Carroll et al. (1992).

Our results place no useful constraints on  $\Omega_0$ . It is interesting to note the fact, however, that likely values of  $\lambda_0$  and  $\Omega_0$  are positively correlated. This is similar to most cosmological tests, a notable exception being constraints derived from CMB anisotropies (see Sect. 5.3). Fortunately, constraints on  $\Omega_0$  from other sources are quite good (Sect. 3.2). Often, this is cast in the form of a constraint on  $\Omega_0 - \lambda_0$  (e.g. Cooray et al. 1999) or, perhaps more practical,  $\lambda_0 - \Omega_0$ . This is a reasonable way of reducing the information to one number, at least when one is concerned with upper limits on  $\lambda_0$  (or  $\lambda_0 - \Omega_0$ ) in a relatively low-density universe. Besides the obvious dependencies on confidence levels and assumptions made, when comparing constraints on  $\lambda_0$  from different investigations one should keep in mind whether they are approximations, like  $\lambda_0 - \Omega_0$  in lensing statistics, and whether a value for a particular scenario (for example, for a flat universe) is the 'obvious' definition or in fact describes the intersection of the  $k = 0$  line with the corresponding 2-dimensional confidence contour, which in general will give a different number. Also, some authors plot 'real' confidence contours while some actually plot contours at values which would correspond to certain confidence contours were the likelihood distribution in the parameter space in question Gaussian.

The left plot in the top row of Fig. 3 shows the joint likelihood of our lensing statistics analysis and that obtained by using conservative estimates for  $H_0$  and the age of the universe (see Sect. 3.2). Although neither method alone sets useful constraints on  $\Omega_0$ , their combination does, since the constraint involving  $H_0$  and the age of the universe only allows large values of  $\Omega_0$  for  $\lambda_0$  values which are excluded by lens statistics. Even though the 68% contour still allows almost the entire  $\Omega_0$  range, it is obvious from the grey scale that much lower values of  $\Omega_0$  are favoured by the joint constraints. The upper limit on  $\lambda_0$  changes only slightly while, as is to be expected, the lower limit

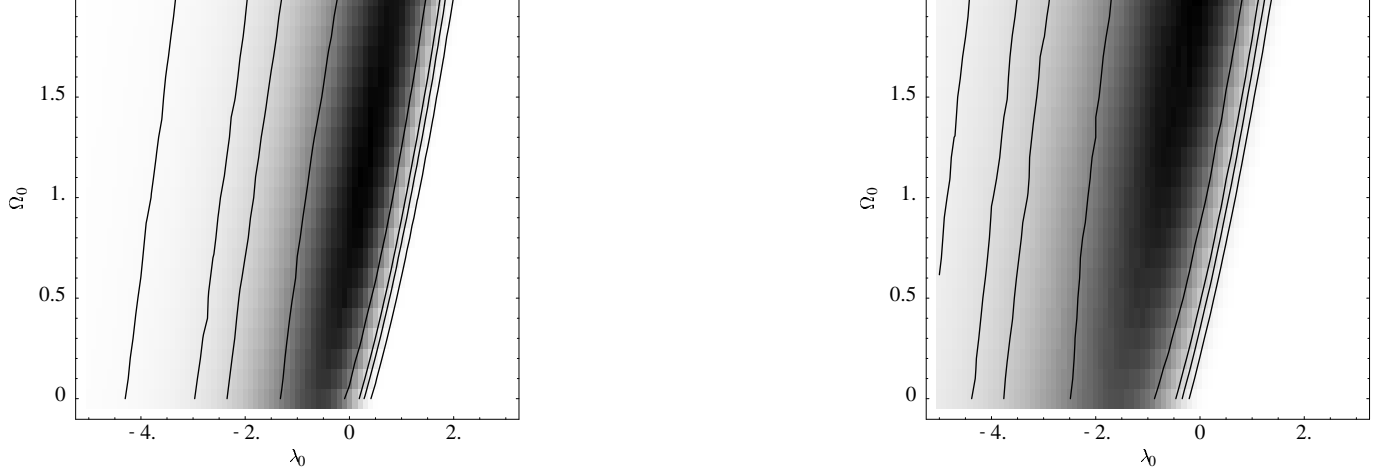


**Fig. 2.** *Left panel:* The likelihood function  $p(D|\lambda_0, \Omega_0, \xi_0)$ . All nuisance parameters are assumed to take precisely their mean values. The pixel grey level is directly proportional to the likelihood ratio, darker pixels reflect higher ratios. The pixel size reflects the resolution of our numerical computations. The contours mark the boundaries of the minimum 0.68, 0.90, 0.95 and 0.99 confidence regions for the parameters  $\lambda_0$  and  $\Omega_0$ . *Right panel:* Exactly the same as the left panel, but the parameter  $n_e$  is increased by two standard deviations

becomes tighter. Also, the change caused by increasing  $n_e$  by 2 standard deviations is less pronounced, with regard to both lower and upper limits on  $\lambda_0$ , as demonstrated in the right plot in top row of Fig. 3.

The middle row of Fig. 3 shows the effect of including our prior information on  $\Omega_0$  (see Sect. 3.2). As is to be expected, (for both values of  $n_e$ ) lower values of  $\Omega_0$  are favoured. This has the side effect of weakening our lower limit on  $\lambda_0$  (though only slightly affecting the upper limit).

We believe that the left plot of the bottom row of Fig. 3 represents very robust constraints in the  $\lambda_0$ - $\Omega_0$  plane. The upper limits on  $\lambda_0$  come from gravitational lensing statistics, which, due to the extremely rapid increase in the optical depth for larger values of  $\lambda_0$ , are quite robust and relatively insensitive to uncertainties in the input data (compare the left and right columns of Fig. 3) as well as to the prior information used data (compare the upper, lower and middle rows of Fig. 3). The upper and lower limits on  $\Omega_0$  are based on a number of different methods and appear to be quite robust, as discussed in Sect. 3.2. The combination of the relatively secure knowledge of  $H_0$  and the age of the universe combine with lens statistics to produce a good lower limit on  $\lambda_0$ , although this is to some extent still subject to the caveats mentioned above.

If one is interested in the allowed range of  $\lambda_0$ , one can marginalise over  $\Omega_0$  to obtain a probability distribution for  $\lambda_0$ . This is illustrated in Fig. 4 and Table 2.

### 5.3. Comparison with other results

For comparison with other results, as a first step one can examine the allowed range of  $\lambda_0$  for the current ‘best-fit’ value for  $\Omega_0$ , which we take, based on the work cited

in Sect. 3.2, to be  $\Omega_0 = 0.3$ . (A more conservative estimate is reflected by using the prior probability distribution  $p_2(\lambda_0, \Omega_0) = L(\Omega_0|0.4, 0.2)$  as shown by the dark grey curve in Fig. 4 and in Table 2.) On the other hand, previous limits on  $\lambda_0$  have often been quoted for a flat universe (K96 and references therein). We consider both cases in Tables 3 and 4.

We do not do a comparison for the special case  $\lambda_0 = 0$  since this analysis of gravitational lensing statistics does not usefully constrain  $\Omega_0$  (any limits coming only from the prior information on  $\Omega_0$ ).

It is beyond the scope of this paper to do a full comparison of different cosmological tests. Except for a few general comments, we therefore restrict ourselves to comments on the similarities and differences between the results from this work without using prior information on  $\lambda_0$  and  $\Omega_0$ , i.e. (the left plot in) Fig. 2, and the those from K96 and Falco et al. (1998) (using only optical data, i.e. the lower left plot in their Fig. 5).

Taking all results at face value and examining the  $\Omega_0 = 0.3$  case first, we note that with ‘three-and-one-half’ exceptions (counting as one test each the four from this work and the three from Falco et al. (1998)) the 68% c.l. *lower* limit from Lineweaver (1998) is *higher* than *all* 68% *upper* limits from other tests, while the 95% lower and upper confidence levels from Lineweaver (1998) are higher than the corresponding limits from the other tests for all but one of these. Even at the 99.9% confidence level (not shown in Table 3), the Lineweaver (1998) result requires  $\lambda_0 \geq 0.12$ . If one assumes  $\Omega_0 = 0.3$ , only Lineweaver (1998) requires  $\lambda_0 > 0$ , though all other tests (except Carlberg (1998)) are compatible with this. This is not surprising, since it is well-known that constraints from



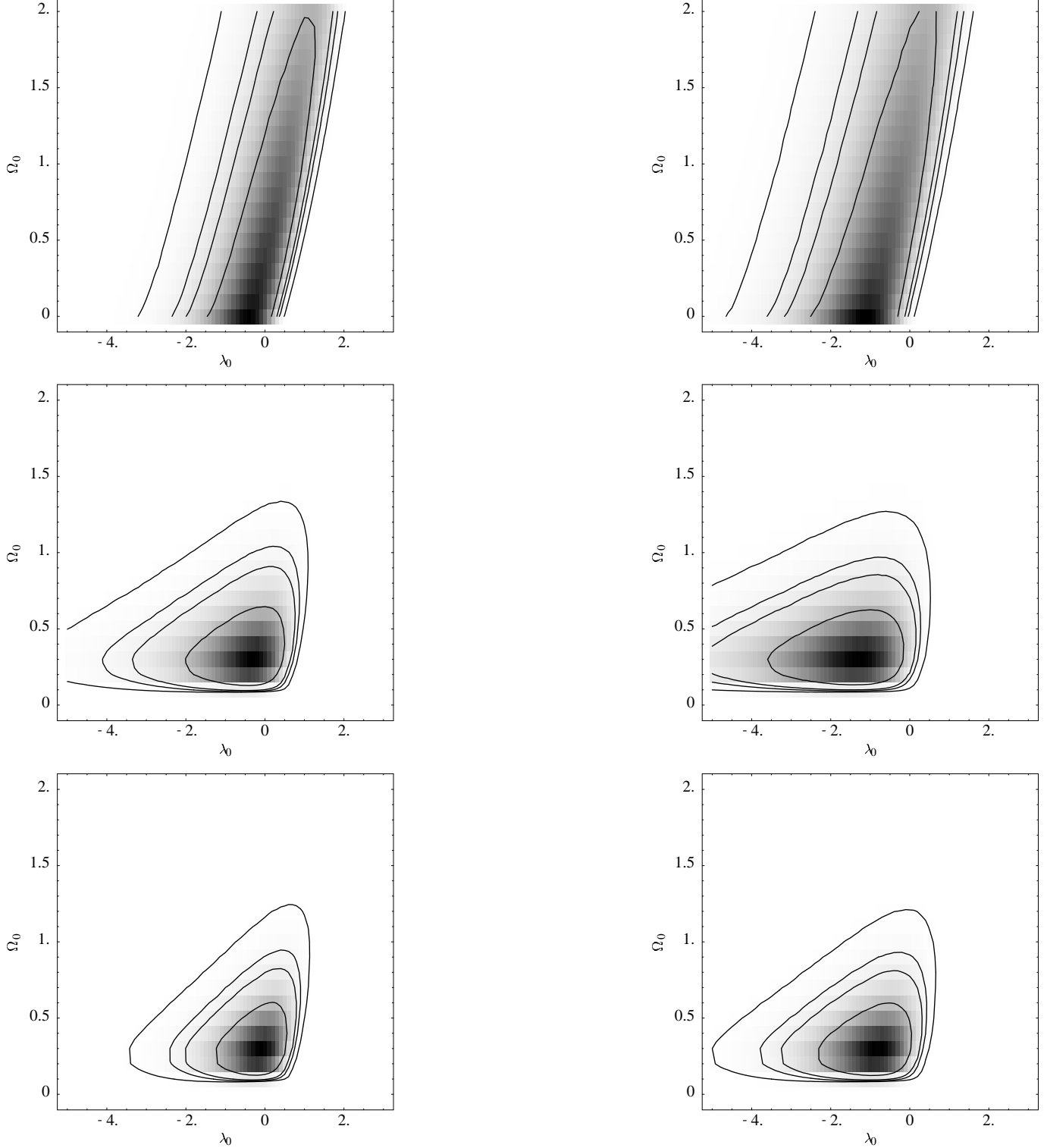


**Fig. 3.** *Left column:* The posterior probability density functions  $p_1(\lambda_0, \Omega_0|D)$  (top panel),  $p_2(\lambda_0, \Omega_0|D)$  (middle panel) and  $p_3(\lambda_0, \Omega_0|D)$  (bottom panel). All nuisance parameters are assumed to take precisely their mean values. The pixel grey level is directly proportional to the likelihood ratio, darker pixels reflect higher ratios. The pixel size reflects the resolution of our numerical computations. The contours mark the boundaries of the minimum 0.68, 0.90, 0.95 and 0.99 confidence regions for the parameters  $\lambda_0$  and  $\Omega_0$ . The respective amounts of information (Eq. (29)) obtained from our sample data are  $I_1 = 1.74$ ,  $I_2 = 1.24$  and  $I_3 = 1.74$ . *Right column:* Exactly the same as the left column, but the parameter  $n_e$  is increased by two standard deviations

**Table 2.** Marginal mean values, standard deviations and 0.95 confidence intervals for the parameter  $\lambda_0$  on the basis of the marginal distributions shown in the top row of Fig. 4; ‘information’ refers to Eq. 29

| Distribution       | Mean  | standard deviation | 95% c.l. range |      | information |
|--------------------|-------|--------------------|----------------|------|-------------|
| $p(D \lambda_0)$   | -0.35 | 1.07               | -2.55          | 1.51 |             |
| $p_1(\lambda_0 D)$ | -0.02 | 0.80               | -1.59          | 1.50 | 1.74        |
| $p_2(\lambda_0 D)$ | -0.78 | 0.97               | -2.85          | 0.76 | 1.24        |
| $p_3(\lambda_0 D)$ | -0.34 | 0.67               | -1.72          | 0.79 | 1.74        |

**Table 3.** Mean values and ranges for assorted confidence levels for the parameter  $\lambda_0$  for our a priori and various a posteriori likelihoods from this analysis and from other tests from the literature (using the latest publicly available results) for the special case  $\Omega_0 = 0.3$ . Except where noted, the ranges quoted are the projections of the corresponding confidence contours in the  $\lambda_0$ - $\Omega_0$  plane onto the  $\lambda_0$  axis<sup>a</sup> (as opposed to  $\Omega_0$ -independent estimates, which of course would always give a smaller range), and are of course two-sided, not one-sided, bounds. Values are either those quoted in the references given and/or obtained from figures in those references; inequalities mean that the corresponding confidence contour is to be found in the range indicated by the inequality, e.g.  $< -1.2$  would mean that the corresponding contour level is to be found at  $\lambda_0 < -1.2$ , *not* that the constraint is  $\lambda_0 < -1.2$  at the corresponding confidence level. This arises because the corresponding area of parameter space was not examined in the reference in question. If the confidence interval could not be determined from the reference, *both* values in the corresponding column are missing

| Cosmological test                                 | 68% c.l. range                                    |         | 90% c.l. range |         | 95% c.l. range |        | 99% c.l. range |        |
|---|---|---------|----------------|---------|----------------|--------|----------------|--------|
| this work, $p(D \lambda_0)$                       | -1.18   | 0.24    | -2.19          | 0.50    | -2.81          | 0.60   | -4.16          | 0.73   |
| this work, $p_1(\lambda_0 D)$                     | -0.97   | 0.46    | -1.55          | 0.60    | -1.89          | 0.69   | -2.73          | 0.81   |
| this work, $p_2(\lambda_0 D)$                     | -2.00   | 0.49    | -3.33          | 0.65    | -4.10          | 0.72   | < -5.00        | 0.80   |
| this work, $p_3(\lambda_0 D)$                     | -1.20   | 0.52    | -1.98          | 0.69    | -2.35          | 0.77   | -3.40          | 0.86   |
| lens statistics (K96)                             | not possible since only $k = 0$ models considered |         |                |         |                |        |                |        |
| radio lenses <sup>b,c</sup>                       | -0.54   | 0.28    | < -1.00        | 0.75    | < -1.00        | 0.89   |                |        |
| optical lenses <sup>d,e</sup>                     | < -1.00   | 0.37    | < -1.00        | 0.75    | < -1.00        | 0.89   |                |        |
| radio + optical lenses <sup>f,g</sup>             | < -1.00   | -0.12   | < -1.00        | 0.50    | < -1.00        | 0.70   | < -1.00        | 0.89   |
| supernovae $m$ - $z$ relation $\mathcal{A}^h$     | -0.70   | 0.50    | -1.15          | 0.75    |                |        |                |        |
| supernovae $m$ - $z$ relation $\mathcal{B}^{ijk}$ | 0.78  | 1.00    |                |         | 0.53           | 1.27   | 0.27           | 1.41   |
| CNOC survey <sup>l</sup>                          | < -0.50   | < -0.50 | < -0.50        | < -0.50 |                |        |                |        |
| CMB <sup>m,n</sup>                                | 0.44  | 0.67    |                |         | 0.36           | > 0.90 | 0.26           | > 0.90 |
| CMB + <i>IRAS</i> <sup>o</sup>                    | not possible since only $k = 0$ models considered |         |                |         |                |        |                |        |
| double radio sources <sup>p</sup>                 | 0.00  | 1.00    | < -2.00        | 1.39    |                |        |                |        |

<sup>a</sup> Note that some references quote confidence ranges for  $k = 0$ —in general, these will be different than the projection of the intersection of the corresponding contour in the  $\lambda_0$ - $\Omega_0$  plane onto the  $\lambda_0$ -axis.

<sup>b</sup> Falco et al. (1998)

<sup>c</sup> contour at 95.4% not 95%

<sup>d</sup> Falco et al. (1998)

<sup>e</sup> contour at 95.4% not 95%

<sup>f</sup> Falco et al. (1998)

<sup>g</sup> contour at 95.4% not 95%

<sup>h</sup> Perlmutter et al. (1998)

<sup>i</sup> Riess et al. (1998)

<sup>j</sup> Fig. 6, solid contours

<sup>k</sup> contours at 68.3%, 95.4% and 99.7% instead of 68%, 95% and 99% respectively

<sup>l</sup> Carlberg (1998)

<sup>m</sup> Lineweaver (1998)

<sup>n</sup> contours at 68.3%, 95.4% and 99.7% instead of 68%, 95% and 99%, respectively

<sup>o</sup> Webster et al. (1998)

<sup>p</sup> Guerra et al. (1998)

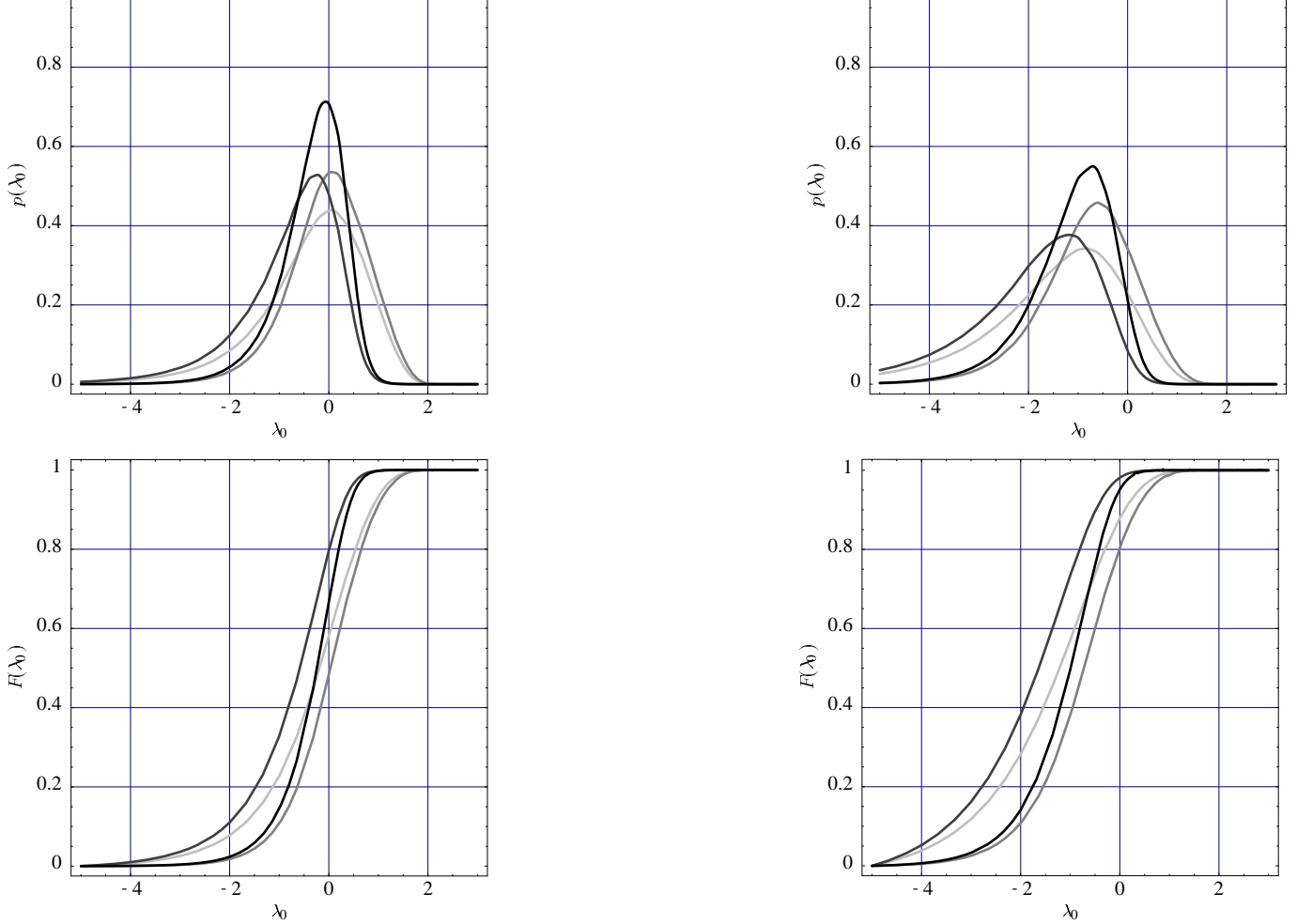


**Fig. 4.** *Left column:* The top panel shows the normalised marginal likelihood function  $p(\lambda_0|D)$  (light grey curve) and the marginal posterior probability density functions  $p_1(D|\lambda_0)$  (medium grey curve),  $p_2(D|\lambda_0)$  (dark grey curve) and  $p_3(D|\lambda_0)$  (black curve). All nuisance parameters are assumed to take precisely their mean values. The bottom panel shows the respective cumulative distribution functions. These can be used to construct any desired  $\Omega_0$ -averaged upper or lower limits on  $\lambda_0$ . *Right column:* Exactly the same as the left column, but the parameter  $n_e$  is increased by two standard deviations

CMB anisotropies tend to run more or less orthogonal in the  $\lambda_0$ - $\Omega_0$  plane to those from most other tests (e.g. White 1998; Eisenstein et al. 1998b; Tegmark et al. 1998a,b).

Examining the  $k = 0$  case, it is interesting to note that the 68% (90%) confidence level *lower* limit on  $\lambda_0$  from Carlberg (1998) is *higher* than *all* of the 68% (90%) c.l. *upper* limits from *all* other tests except Guerra et al. (1998). Otherwise, with ‘one-and-one-half’ exceptions all tests are compatible even at the 68% confidence level. If one assumes  $k = 0$ , then the evidence for  $\lambda_0 > 0$  looks convincing: at the 68% confidence level, again with ‘one-and-one-half’ exceptions, all tests indicate  $\lambda_0 > 0$ ; even at 90% the evidence is still quite good, if one keeps in mind that the gradient towards smaller values of  $\lambda_0$  is generally not as steep as towards larger values.

Again taken at face value, neither the  $k = 0$  case nor the  $\Omega_0 = 0.3$  case are compatible with all tests, even at the

$\approx 90\%$  confidence level. It appears the simplest solution to achieve concordance would be to have  $\Omega_0 \approx 0.2$ , which is within the error on  $\Omega_0$  discussed in Sect. 3.2. For  $k = 0$  this would imply  $\lambda_0 = 0.8$ , which seems to be ruled out, thus ruling out the flat universe altogether. For a non-flat universe, reducing  $\Omega_0$  would, due to the CMB constraint, require a higher value of  $\lambda_0$ , and thus make the  $\lambda_0 = 0$  case more unlikely, ruling out this special case as well.

On balance, a cosmological model with  $\lambda_0 \approx 0.3$  and  $\Omega_0 \approx 0.25$  seems compatible with all known observational data (not just those discussed here) at a comfortable confidence level.

For a ‘likely’  $\Omega_0$  value of 0.3 we have calculated the likelihood with the higher resolution  $\Delta\lambda_0 = 0.01$ . This is shown in Fig. 5. From these calculations one can extract confidence limits which, due to the higher resolution in

**Table 4.** Mean values and ranges for assorted confidence levels for the parameter  $\lambda_0$  for our a priori and various a posteriori likelihoods from this analysis and from other tests from the literature (using the latest publicly available results) for the special case  $k = 0$ . Otherwise the same as Table 3, in particular the references are not listed in the footnotes to this table.  $X$  denotes the fact that there is no intersection of the confidence contour with the  $k = 0$  line

| Cosmological test                                | 68% c.l. range |      | 90% c.l. range |        | 95% c.l. range |        | 99% c.l. range |        |
|--|----------------|------|----------------|--------|----------------|--------|----------------|--------|
| this work, $p(D \lambda_0)$                      | -0.68          | 0.51 | < -1.00        | 0.57   | < -1.00        | 0.62   | < -1.00        | 0.70   |
| this work, $p_1(\lambda_0 D)$                    | -0.09          | 0.56 | -0.38          | 0.64   | -0.57          | 0.68   | -1.04          | 0.81   |
| this work, $p_2(\lambda_0 D)$                    | $X$            | $X$  | 0.09           | 0.69   | -0.03          | 0.73   | -0.28          | 0.92   |
| this work, $p_3(\lambda_0 D)$                    | 0.47           | 0.48 | 0.18           | 0.67   | 0.07           | 0.70   | -0.14          | 0.84   |
| lens statistics <sup>a</sup>                     |                |      |                |        | < 0.00         | 0.66   |                |        |
| radio lenses <sup>b</sup>                        | -0.47          | 0.56 | < -1.00        | 0.72   | < -1.00        | 0.80   | < -1.00        | 0.85   |
| optical lenses <sup>c</sup>                      | < -1.00        | 0.56 | < -1.00        | 0.72   | < -1.00        | 0.80   | < -1.00        | 0.87   |
| radio + optical lenses <sup>d</sup>              | -0.87          | 0.43 | < -1.00        | 0.60   | < -1.00        | 0.69   | < -1.00        | 0.78   |
| supernovae $m$ - $z$ relation $\mathcal{A}$      | 0.20           | 0.60 | -0.05          | 0.75   |                |        |                |        |
| supernovae $m$ - $z$ relation $\mathcal{B}^{ef}$ | 0.74           | 0.83 |                |        | 0.61           | 0.92   | 0.50           | 1.00   |
| CNO survey                                       | 0.85           | 0.95 | 0.81           | 0.98   |                |        |                |        |
| CMB <sup>g</sup>                                 | < 0.00         | 0.60 | < 0.00         | < 0.00 | < 0.00         | < 0.00 | < 0.00         | < 0.00 |
| CMB + $IRAS^h$                                   | 0.47           | 0.71 |                |        |                |        |                |        |
| double radio sources                             | 0.35           | 1.00 | 0.70           | 1.00   |                |        |                |        |

<sup>a</sup> value for  $k = 0$ , not projection

<sup>b</sup> contour at 95.4% not 95%

<sup>c</sup> contour at 95.4% not 95%

<sup>d</sup> contour at 95.4% not 95%

<sup>e</sup> Fig. 6, solid contours

<sup>f</sup> contours at 68.3%, 95.4% and 99.7% instead of 68%, 95% and 99% respectively

<sup>g</sup> contour at 68.3% instead of 68%; other contours, and part of the 68.3% contour, lie partially in the  $k = +1$  area of parameter space which was not examined for technical reasons in Lineweaver (1998)

<sup>h</sup> value for  $k = 0$ , not projection

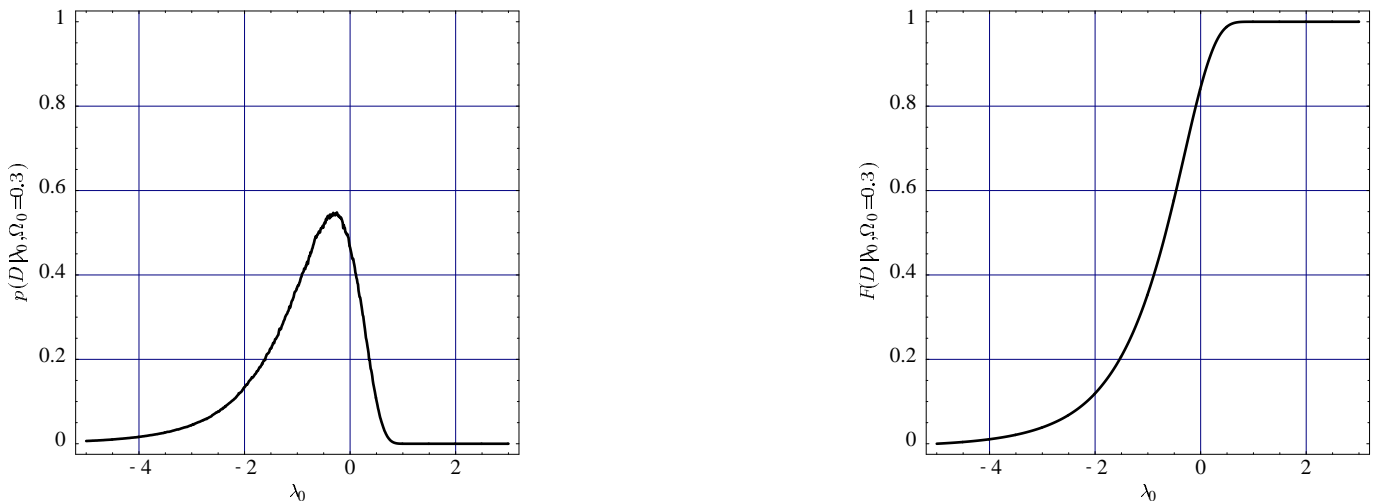


**Fig. 5.** *Left panel:* The likelihood function as a function of  $\lambda_0$  for  $\Omega_0 = 0.3$  and with all nuisance parameters taking their default values. *Right panel:* The same but plotted cumulatively. See Table 5

**Table 5.** Confidence ranges for  $\lambda_0$  assuming  $\Omega_0 = 0.3$ . Unlike the results presented in Table 3, these figures are for a specific value of  $\Omega_0$  and not the values of intersection of particular contours with the  $\Omega_0 = 0.3$  line in the  $\lambda_0$ - $\Omega_0$  plane. These are more appropriate if one is convinced that  $\Omega_0 = 0.3$  and have been calculated using ten times better resolution than the rest of our results presented in this work. See Fig. 5

| 68% c.l. range |      | 90% c.l. range |      | 95% c.l. range |      | 99% c.l. range |      |
|----------------|------|----------------|------|----------------|------|----------------|------|
| -1.27          | 0.27 | -2.26          | 0.51 | -2.87          | 0.60 | -4.10          | 0.72 |

should be compared to those for  $p(D|\lambda_0)$  from Table 3.

Again, a full discussion of joint constraints involving discussion of possible sources of error for each test, as well as comparing the full contours in the  $\lambda_0$ - $\Omega_0$  plane, is beyond the scope of this paper. However, quick comparisons would be aided were the results of all tests available in an easy-to-process electronic form (see below); such quick consistency tests would enable one to spot areas of inconsistency much more quickly. Also, it should be emphasised that the projections onto the  $\lambda_0$ -axis of the intersection of a particular confidence contour with the  $\Omega_0 = 0.3$  or  $k = 0$  axis are generally *not* the same as the corresponding confidence interval for the  $\Omega_0 = 0.3$  or  $k = 0$  special cases.

For a flat universe, our 95% confidence level upper limit on  $\lambda_0$ - $\Omega_0$ , i.e. the value of  $\lambda_0$  where this contour crosses the  $k = 0$  line, is  $\lambda_0 < 0.62$ . This is essentially the same as the  $\lambda_0 < 0.66$  of K96, as was to be expected considering we used essentially the same data and methods. Interpreted cautiously, one might conclude from this that the singular isothermal sphere model is a good approximation as far as determining the cosmological parameters from lens statistics is concerned, as was assumed in Falco et al. (1998). Our 99% confidence level upper limit on  $\lambda_0$  is  $\lambda_0 < 0.70$ . This is quite a tight upper bound on  $\lambda_0$  and appears to be quite robust.

Perhaps more interesting is the comparison with (the results using only optical data in) Falco et al. (1998). Although a detailed comparison is complicated by the different plotting scheme and reducing the entire contour (or indeed grey-scale) plot to a few numbers throws away information, it is obvious that the plots are broadly similar. Our 68% contour is, for  $\Omega_0 \approx 1$ , roughly parallel to the  $\lambda_0$ -axis at  $\lambda_0 \approx -1$ . This is just at the edge of the Falco et al. (1998) plot, and as they provide no grey-scale, it is difficult to compare the lower limits on  $\lambda_0$ . Thus, while our main goal was to explore a ‘large enough’ region of parameter space, comparison in the areas where there is overlap shows consistency, which strengthens our faith in the conclusions pertaining to areas of parameter space where there is no overlap.

Recently, it has become quite fashionable to discuss joint constraints derived from a variety of cosmological tests. This has grown from plotting the overlap of likelihood contours (often in a space spanned by parameters other than  $\lambda_0$  and  $\Omega_0$ ) (e.g. Ostriker & Steinhardt 1995; Turner 1996; Bagla et al. 1996; Krauss 1998; White 1998) to full-blown joint likelihood analyses, both detailed theoretical investigations of what will be possible in the future (e.g. Tegmark et al. 1998a,b; Eisenstein et al. 1998a,b) and more restricted analyses using present data (e.g. Webster et al. 1998). While in some cases it is quick and easy to calculate the likelihood as a function of  $\lambda_0$  and  $\Omega_0$  given the data, for example for tests using the  $m$ - $z$  relation, in other cases such as the present one it is a major programming and computational effort to do so. To aid comparisons, all

of numbers at

[http://multivac.jb.man.ac.uk:8000/ceres/data\\_from\\_papers/lower\\_limit.html](http://multivac.jb.man.ac.uk:8000/ceres/data_from_papers/lower_limit.html)

and we urge our colleagues to follow our example. We applaud the fact that most results are now presented in the  $\lambda_0$ - $\Omega_0$  plane, as opposed to using other parameters such as  $q_0$  or  $\Omega_{\text{tot}} \equiv \lambda_0 + \Omega_0$ . A further aid in comparison would be a uniform choice of axes. We prefer to plot  $\Omega_0$  on the  $y$ -axis and  $\lambda_0$  on the  $x$  axis since up/down symmetry is less fundamental than left/right symmetry and this mirrors the fact that  $\Omega_0$  has the physical lower limit  $\Omega_0 = 0$  whereas no corresponding upper or lower limits for  $\lambda_0$  exist. Square plots with the same range would further aid the comparison. Of course, if all data are publicly available, then they can be re-plotted to taste.

## 6. Summary and conclusions

We have re-analysed optical gravitational lens surveys from the literature, using the techniques described in Kochanek (1996), for the first time allowing both the cosmological constant  $\lambda_0$  and the density parameter  $\Omega_0$  to be free parameters while also using a non-singular lens model. We confirm the well-known results that gravitational lensing statistics can provide a good upper limit on  $\lambda_0$  but are relatively insensitive to  $\Omega_0$ . We have presented the new result of a robust lower limit on  $\lambda_0$ , which is a substantial improvement on previously known *robust* lower limits. Coupled with relatively conservative prior information about the Hubble constant  $H_0$ , the age of the universe and the well-established value of  $\Omega_0$ , one can reduce the allowed parameter space in the  $\lambda_0$ - $\Omega_0$  plane to a small, finite region, which is similar to the area allowed by joint constraints based on many other cosmological tests (see Fig. 3).

Using lens statistics information alone, at 95% confidence, our lower and upper limits on  $\lambda_0 - \Omega_0$  are respectively  $-3.17$  and  $0.3$ . For a flat universe, this corresponds to lower and upper limits on  $\lambda_0$  of respectively  $-1.09$  and  $0.65$ . Keeping in mind the difficulties of a quantitative comparison, this is in good agreement with other recent measurements of the cosmological constant. This value was calculated from Table 5 and assuming a degeneracy in  $\lambda_0 - \Omega_0$  as in Cooray et al. (1999) and Cooray (1999). For comparison, from Table 4, the corresponding value for the upper limit on  $\lambda_0$  is  $0.62$  and the value from K96 is  $0.66$ .<sup>5</sup>

For detailed comparison of cosmological tests, one needs to compare confidence contours—calculated in the same,

<sup>5</sup> The value from Cooray et al. (1999) and Cooray (1999) is  $0.79$ , but it should be noted this value (the same in both papers) is based on different surveys, namely the Hubble Deep Field and CLASS, respectively.)

Of course, this makes it difficult to meaningfully reduce the results of a given cosmological test to one or even a few single numbers. Unless a cosmological test is developed which can measure  $\lambda_0$  independently of any other parameters, there is not much point in quoting unqualified ‘limits on  $\lambda_0$ ’.

Presently tentative claims of the detection of a positive cosmological constant, if true, would rank among the great discoveries of cosmology. Even though there are serious difficulties involved, it seems worthwhile to be able to confirm this result by improving the lower limit on  $\lambda_0$  derived from gravitational lensing statistics. Targetting the two primary sources of uncertainty calls for improving our knowledge of the normalisation of the local luminosity density of galaxies as well as increasing the size of gravitational lens surveys. As far as the latter goes, the CLASS survey (Browne et al. 1998; Myers et al. 1999) looks the most promising at the moment. In a companion paper (Helbig et al. 1999), we have shown that comparable constraints to the ones presented in this work can be obtained from the JVAS gravitational lens survey; this gives us hope that the much larger CLASS survey will offer improvement in this area.

Cosmological tests which set tight upper limits on  $\Omega_0$  imply, for a flat  $k = 0$  universe, a value of  $\lambda_0$  which is ruled out by lensing statistics. For a non-flat universe, many tests are indicating  $\lambda_0 > 0$ , and at present a cosmological model with  $\lambda_0 \approx 0.3$  and  $\Omega_0 \approx 0.25$  seems compatible with all known observational data, with neither a flat universe nor a universe without a positive cosmological constant being viable alternatives. The simplest case, the Einstein-de Sitter universe with  $\lambda_0 = 0$  and  $\Omega_0 = 1$ , both flat and without a cosmological constant, had been abandoned long before the new observational data cited in this work came to light (see, e.g., Ostriker & Steinhardt 1995, and references therein); this trend has continued, with the next-most-simple cases also no longer viable. For  $\lambda_0$  and  $\Omega_0$ , we have in a sense reached the least simple case; it will be interesting to see if this trend continues with regard to the other cosmological parameters, in particular those which can be measured by the *Planck Surveyor* mission. Larger gravitational lens surveys such as CLASS will be a step in this direction.

*Acknowledgements.* We thank Sjur Refsdal, Leon Koopmans, Lutz Wisotzki and many colleagues at Jodrell Bank for helpful comments and suggestions. This research was supported in part by the European Commission, TMR Programme, Research Network Contract ERBFMRXCT96-0034 ‘CERES’.

## Appendix A: Getting a feel for it

The likelihood of a given cosmological model for a given set of observational data, calculated using Eq. (3), is the result of the complex interplay of many factors. While this

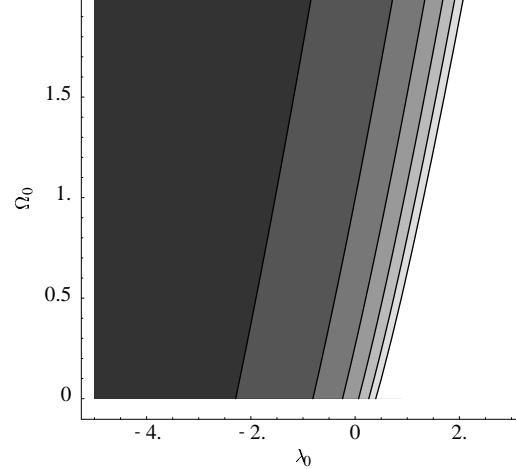


**Fig. A1.** Likelihood that the non-lenses in our sample are not lenses. The contour levels mark changes of a factor of ten in the probability, which is also indicated by the grey scale, darker values corresponding to higher values

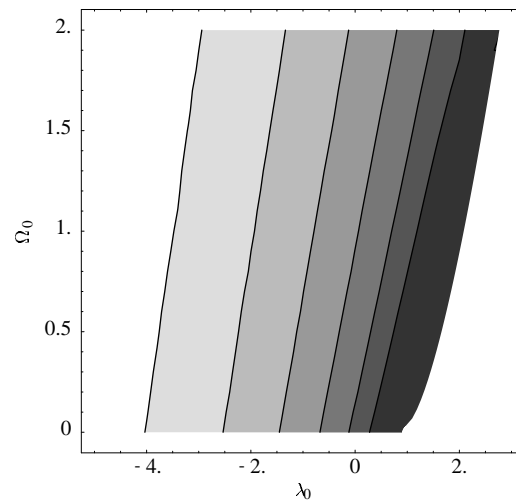


**Fig. A2.** Likelihood that the lenses in our sample have the properties they do. The contour levels mark changes of a factor of ten in the probability, which is also indicated by the grey scale, darker values corresponding to higher values

is necessary for a detailed analysis, it perhaps obscures the fact that the likelihood is basically the product of two terms, the likelihood that the non-lenses in our sample are not lenses (see Fig. A1) and the likelihood that the lenses in our sample (see Fig. A2) have the observed properties.<sup>6</sup>

<sup>6</sup> It is interesting to note that the measurement of  $\lambda_0$  by Im et al. (1997) (who obtain  $\lambda_0 = 0.64^{+0.15}_{-0.26}$  for a flat universe and thus a lower limit) essentially corresponds to Fig. A2 (though with a different sample of lenses). Since lensing is a rare phenomenon, small-number statistics are a source of concern. The advantage of a well-defined *gravitational lens survey*, as opposed to using a ‘sample from the literature’, is that the (much greater) number of non-lenses in the sample also makes

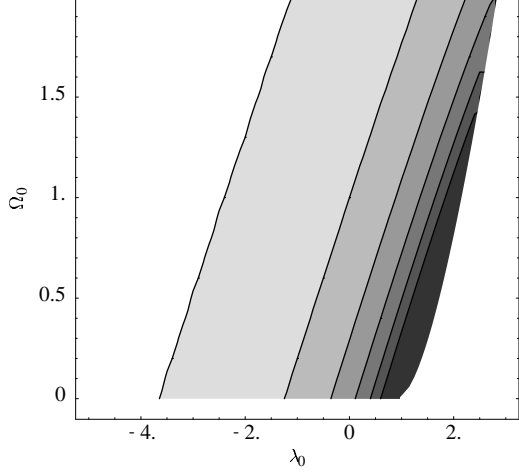


**Fig. A3.** The volume element  $dV/dz$  at the typical lens galaxy redshift  $z_d = 0.7$ . The contours indicate the fraction 0.1, 0.2, ... 0.6 of the volume element in the limiting case of the de Sitter model ( $\lambda_0 = 1, \Omega_0 = 0$ ). This is also indicated by the grey scale, darker values corresponding to a larger volume. For smaller redshifts the contours are more vertical (and further apart), for larger redshifts more horizontal (cf. Fig. 3 of Tegmark et al. (1998b) but note their swapped axes)

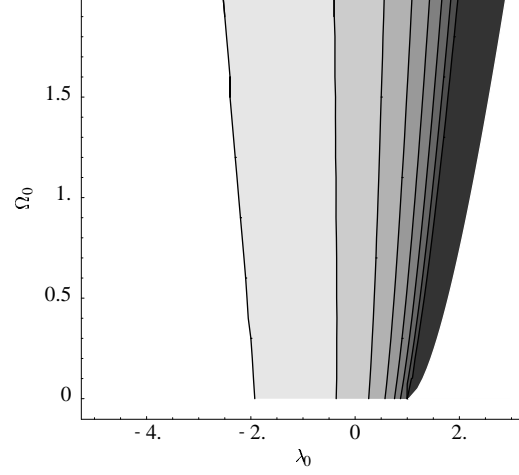


**Fig. A4.** Cross section for the softened singular isothermal sphere model used in this work for a typical lens redshift  $z_d = 0.7$  and a typical source redshift  $z_s = 2.0$  for the fiducial values  $\sigma = \sigma_*$  and  $s = s_*$  (see Sect. 4). The contours indicate the fraction 0.3, 0.4, ... 1.0 of the cross section in the limiting case of the de Sitter model ( $\lambda_0 = 1, \Omega_0 = 0$ ). This is also indicated by the grey scale, darker values corresponding to a larger cross section

The latter in turn is the result of two basic effects: the dependency of the volume element  $dV/dz$  on  $\lambda_0$  and  $\Omega_0$  (see Fig. A3) and the dependency on the lensing cross section on  $\lambda_0$  and  $\Omega_0$  (see Fig. A4). One can also use the probability that the non-lenses in our sample are not lenses (illustrated in Fig. A1) to calculate the expected number of lenses in our sample (see Fig. A5), although obviously just counting the number of lenses does not make use of as much of the available information as does using Eq. (3).

## References

Bagla J.S., Padmanabhan T., Narlikar J.V., 1996, *Comments Astrophys.*, 18, 275  
 Bahcall N., Fan X., Cen R., 1997, *ApJ*, 485, L53  
 Bahcall N.A., 1998, In: Müller et al. (1998), pp. 137–146, [astro-ph/9711062](#)  
 Barrow J.D., 1995, *Phys. Rev. D*, 51, 3113  
 Bartelmann M., Huss A., Colberg J.M., Jenkins A., Pearce F.R., 1998, *A&A*, 330, 1  
 Bernardo J.M., Smith A.F.M., 1994, *Bayesian Theory*. Wiley, New York  
 Browne I.W.A., Jackson N.J., Augusto P., et al., 1998, In: *Observational Cosmology with the new Radio Surveys*, Kluwer Academic Publishers, Dordrecht, pp. 323–32  
 Carlberg R.G., 1998, In: Thanh & Giraud-Heraud (1998), pp. 423–7, [astro-ph/9804329](#)

a contribution. A comparison of Figs. A1 and A2 hints that not taking the non-lenses into account would tend to favour a high value of  $\lambda_0$ , as indeed found by Im et al. (1997).

Carlberg R.G., Yee H.K.C., Ellingson E., et al., 1998a, In: Thanh & Giraud-Heraud (1998), pp. 279–82, [astro-ph/9804312](#)  
 Carlberg R.G., Yee H.K.C., Lin H., et al., 1998b, In: Müller et al. (1998), pp. 119–126, [astro-ph/9711272](#)  
 Carlberg R.G., Yee H.K.C., Morris S.L., et al., 1998c, *Phil. Trans. R. Soc. Lond. A*, in press, [astro-ph/9805131](#)  
 Carroll S.M., Press W.H., Turner E.L., 1992, *ARA&A*, 30, 499  
 Chaboyer B., Demarque P., Kernan P.J., Krauss L.M., 1998, *ApJ*, 494, 96  
 Cheng Y.C.N., Krauss L.M., 1999, *MNRAS*, submitted, [astro-ph/9810393](#)  
 Coles P., Ellis G.F.R., 1994, *Nat*, 370, 609  
 Coles P., Ellis G.F.R., 1997, *Is the Universe Open or Closed? No. 7* in *Cambridge Lecture Notes in Physics*, Cambridge University Press, Cambridge  
 Collins II G.W., 1997, *Comments Astrophys.*, 18, 353  
 Cooray A.R., 1999, *A&A*, 342, 353  
 Cooray A.R., Quashnock J.M., Miller M.C., 1999, *ApJ*, 511, 562  
 da Costa L.N., Nusser A., Freudling W., et al., 1998, *MNRAS*, 299, 425, 11Sep.  
 Crampton D., McClure R.D., Fletcher J.M., 1992, *ApJ*, 392, 23  
 Czoske O., 1995, *Die kosmologischen Parameter  $\Omega_M$  und  $\Omega_\Lambda$ . Eine Übersicht über Bestimmungsmethoden und Ergebnisse*. Master's thesis, Universität Hamburg  
 Daly R.A., Guerra E.J., Wan L., 1998, In: Thanh & Giraud-Heraud (1998), pp. 323–6, [astro-ph/9803265](#)

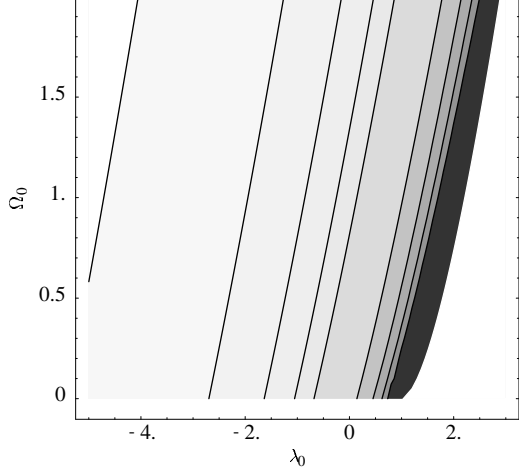


**Fig. A5.** Expected number of lenses. Contours, from left to right, indicate 1, 2, 3, 4, 5, 10, 15, 20 and 25 lenses. Darker values of the grey scale correspond to higher values. Cf. Cooray et al. (1999) and Cooray (1999) where the number of lenses as a function of  $\lambda_0$  and  $\Omega_0$  has been calculated for the Hubble Deep Field and for CLASS

Eisenstein D.J., Hu W., Tegmark M., 1998a, ApJ, 504, L57  
Eisenstein D.J., Hu W., Tegmark M., 1998b, ApJ, in press, **astro-ph/9807130**  
Falco E., Kochanek C.S., Muñoz J.A., 1998, ApJ, 494, 47  
Fan X., Bahcall N., Cen R., 1997, ApJ, 490, L123  
Favati P., Lotti G., Romani F., 1991a, ACM Trans. Math. Softw., 17, 207  
Favati P., Lotti G., Romani F., 1991b, ACM Trans. Math. Softw., 17, 218  
Feige B., 1992, Astron. Nachr., 313, 139  
Franx M., van Dokkum P., Illingworth G.D., Kelson D.D., Tran K.V., 1998, In: D'Odorico S., Fontana A., Giallongo E. (eds.), The Young Universe: Galaxy Formation and Evolution at Intermediate and High Redshift, Astronomical Society of the Pacific, vol. 146 of ASP Conference Series, p. 142  
Fukugita M., Futamase T., Kasai M., 1990, MNRAS, 246, 24  
Fukugita M., Futamase K., Kasai M., Turner E.L., 1992, ApJ, 393, 3  
Gott III J.R., Gunn J.E., Schramm D.N., Tinsley B., 1974, ApJ, 194, 543  
Gott III J.R., Park M.G., Lee H.M., 1989, ApJ, 338, 1  
Guerra E.J., Daly R.A., Wan L., 1998, ApJ, submitted, **astro-ph/9807249**  
Guth A.H., 1981, Phys. Rev. D, 23, 347  
Helbig P., Marlow D.R., Quast R., et al., 1999, AAS, 136, 297  
Hinshaw G., Krauss L.M., 1987, ApJ, 320, 468  
Im M., Griffiths R.E., Ratnatunga K.U., 1997, ApJ, 475, 457

1995, A&A, 300, 323  
Kayser R., Helbig P., Schramm T., 1997, A&A, 318, 680  
Kochanek C.S., 1993, ApJ, 419, 12  
Kochanek C.S., 1996, ApJ, 466, 638  
Kochanek C.S., Falco E.E., Schild R., 1995, ApJ, 452, 109  
Kochanek C.S., Falco E.E., Impey C., et al., 1997, <http://cfa-www.harvard.edu/glensdata/>  
Krauss L.M., 1998, ApJ, 501, 461  
Lineveaver C.H., 1998, ApJ, 505, L69  
Maoz D., Bahcall J.N., Schneider D.P., et al., 1993, ApJ, 409, 128  
Martel H., Shapiro P.R., Weinberg S., 1998, ApJ, 492, 29  
Matravers D.R., Ellis G.F.R., Stoeger W.R., 1995, QJRAS, 36, 29  
Müller V., Gottlöber S., Mucket J.P., Wambsganß J. (eds.), 1998, Large Scale Structure: Tracks and Traces. Proceedings of the 12th Potsdam Cosmology Workshop, Potsdam Cosmology Workshops, Singapore, World Scientific  
Myers S.T., Rusin D., Marlow D., et al., 1999, in preparation  
Ostriker J.P., Steinhardt P.J., 1995, Nat, 377, 600  
Park M.G., Gott III J.R., 1997, ApJ, 489, 476  
Peebles P.J.E., 1993, Principles of Physical Cosmology. Princeton University Press, Princeton  
Penrose R., 1989, In: Fenyves E.J. (ed.), Fourteenth Texas Symposium on Relativistic Astrophysics, New York Academy of Sciences, New York, vol. 571, pp. 249–264  
Perlmutter S., Aldering G., Valle M.D., et al., 1998, Nat, 391, 51  
Riess A.G., Filippenko A.V., Challis P., et al., 1998, AJ, 116, 1009  
Schmidt B.P., Suntzeff N.B., Phillips M.M., et al., 1998, ApJ, 507, 46  
Schneider P., Ehlers J., Falco E.E., 1992, Gravitational Lenses. Springer-Verlag, Heidelberg  
Tegmark M., Eisenstein D.J., Hu W., 1998a, In: Thanh & Giraud-Heraud (1998), pp. 355–8, **astro-ph/9804168**  
Tegmark M., Eisenstein D.J., Hu W., Kron R.G., 1998b, ApJ, submitted, **astro-ph/9805117**  
Thanh J.T., Giraud-Heraud Y. (eds.), 1998, Fundamental Parameters in Cosmology, Proceedings of the XXXIIIrd Rencontres de Moriond, Paris, Éditions Frontiers  
Turner E.L., 1990, ApJ, 365, L43  
Turner E.L., Ostriker J.P., Gott III J.R., 1984, ApJ, 284, 1  
Turner M.S., 1996, In: Zichichi A. (ed.), Vacuum and Vacua: The Physics of Nothing, World Scientific, Singapore, p. 50  
Turok N., Hawking S.W., 1998, Phys. Lett. B, 432, 271  
Veron-Cetty M.P., Veron P., 1996, ESO Sci. Rep., 17, 1  
Webster M., Bridle S.L., Hobson M.P., et al., 1998, ApJ, 506, 495  
Yee H.K.C., Filippenko A.V., Tang D.H., 1993, AJ, 105, 7